UCL Mechanical Engineering 2020/2021

MECH0011 Fluid Mechanics Laboratory

Lift of a NACA-0012 Aerofoil

Group 21

Haochen Yang, Muhammad Naveed, Yikai Zhang, Ryan El Khoury, Hasha Dar

January 10, 2021

Introduction to Lift and Drag

Description of lift and drag

A fluid, for example air in our case, that flows around an object will act a force on it. In our case, this object is the airfoil. Lift is the effect of the force applied by the fluid in the perpendicular direction to the flow direction. The lift force can be calculated with known pressure distribution.

$$L = \oint (pnk)\,\mathrm{d}S \tag{1}$$

Where p is the pressure on the surface of the airfoil, n is the normal unit vector pointing into the wing, k is the vertical unit vector, normal to the airfoil direction. Or it can be calculated by using lift coefficient:

$$L = \frac{1}{2}\rho V^2 A C_l \tag{2}$$

Where ρ is the density of the fluid (air), V is the velocity of the flow and A is the wing area. Drag is also called fluid resistance because it acts like a resistance force. Drag acts opposite to the motion of any object with respect to the fluid that flows around it. Drag can also be calculated as:

$$D = \frac{1}{2}\rho V^2 A C_d \tag{3}$$

Where C_d is the drag coefficient.

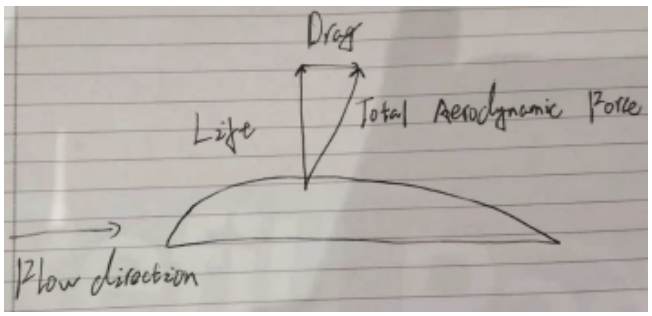

Figure 1:

Description of the difference between form and friction drags, and how their contribution differ in streamlined and bluff bodies

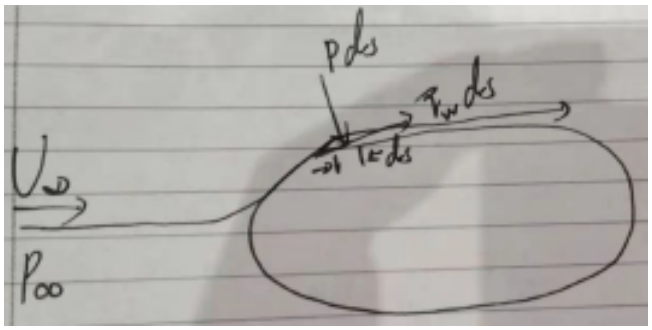

Figure 2:

Force generated by pressure can be written as:

$$F = p\,\mathrm{d}S \tag{4}$$

Where p is the pressure on the surface area $\mathrm{d}S$. Form drag is the normal component of the force normal to the surface. Hence, the form drag can be calculated by integrating the force component in the stream direction iver the whole surface area.

$$D_f = \int_S (p)\,\mathrm{d}S \tag{5}$$

The skin friction is the tangential component of the force normal to the surface. Hence, skin friction can be calculated by integrating the shear force, $\tau_w\,\mathrm{d}S$, over the whole area.

$$F_s = \int_S (\tau_w)\,\mathrm{d}S \tag{6}$$

Determination of the lift coefficient of a finite wing utilising the coefficient of an infinite one. Explanation on why this is necessary and what measures can be taken to improve the efficiency of a wing

The lift coefficient of the finite wing can be calculated with given lift coefficient of a finite wing by using lifting-line theory.

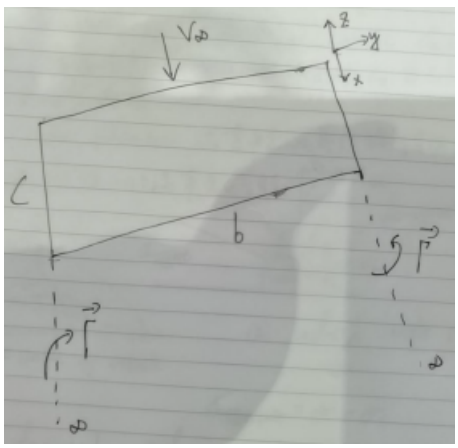

Figure 3: For a given wing with wing span b and chord length c

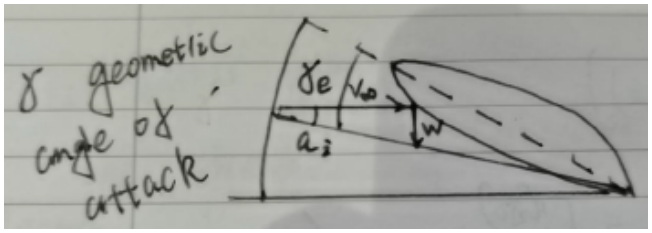

Figure 4:

As shown in the graph, the geometric angle of attack is α and α_e is the effective geometry of angle of attack. α_i is the induced angle of attack. V_∞ is the free stream flow velocity, W is the downwash caused by the flow and $\alpha_e = \alpha - \alpha_i$.

Also, by applying the *Biot-Savart* Law, for a given vortex filament with strength Γ, the velocity of a certain point P which is created by this vortex

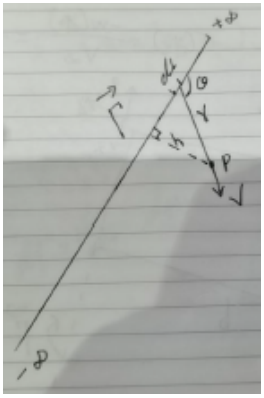

Figure 5:

$$\left|\vec{V}\right| = \frac{\Gamma}{4\pi}\int_{-\infty}^{\infty}\frac{\left|\mathrm{d}\vec{l}\cdot\vec{r}\right|}{|r|^3} \tag{7}$$

$$l = r\cos\theta \tag{8}$$

$$h = r\sin\theta \tag{9}$$

$$\mathrm{d}l = -\frac{h}{\sin\theta} \tag{10}$$

$$\left|\vec{V}\right| = \frac{\Gamma}{4\pi}\int_{\pi}^{0}\left(\frac{-\sin\theta}{h}\right)\mathrm{d}\theta \tag{11}$$

$$\tag{12}$$

So the downwash at a certain point on the wing will be:

$$W = \frac{\Gamma}{4\pi h}\int_{\frac{\pi}{2}}^{0}(-\sin\theta)\,\mathrm{d}\theta = \frac{\Gamma}{4\pi h} \tag{13}$$

The lift per unit span:

$$L_v = \rho V_\infty \Gamma = \frac{1}{2}\rho V_\infty^2 c C_l = \frac{1}{2}\rho V_\infty^2 c \cdot 2\pi\alpha_e \tag{14}$$

$$\Gamma = cV_\infty \pi\left(\alpha - \alpha_i\right) \tag{15}$$

$$\alpha_i = \frac{-w\left(y\right)}{V_\infty} \tag{16}$$

However when we are considering the downwash at the wing tips where $h = 0$. The angle of attack is approach infinity, but that's impossible. So, we introduce the lifting-line theory. We suggest that γ is a function of y. But according to *Helmholtz's* first theorem, the strength of a vortex filament is a constant along its length. So, in order to let Γ to change y along y, we create an infinitely large number of trailing vortexes which all have slightly different strengths.

$$\mathrm{d}\Gamma = \frac{\mathrm{d}\Gamma}{\mathrm{d}y}\,\mathrm{d}y \tag{17}$$

$$\therefore W\left(y_0\right) = \int_{\frac{-b}{2}}^{\frac{b}{2}} \left(\frac{\frac{\mathrm{d}\Gamma}{\mathrm{d}y}}{4\pi\left(y - y_0\right)}\right)\mathrm{d}y \tag{18}$$

$$C_l = \frac{2\Gamma\left(y_0\right)}{V_\infty c\left(y_0\right)} = 2\pi\alpha_e = 2\pi\left(\alpha\left(y_0\right) - \alpha_i\left(y_0\right)\right) \tag{19}$$

$$\alpha_i\left(y_0\right) = -\frac{w\left(y_0\right)}{V_\infty} = -\frac{1}{4\pi V_\infty}\int_{\frac{-b}{2}}^{\frac{b}{2}} \left(\frac{\frac{\mathrm{d}\Gamma}{\mathrm{d}y}\,\mathrm{d}y}{y - y_0}\right) \tag{20}$$

$$\Gamma\left(y\right) = \Gamma\left(y_0\right)\sqrt{1 - \left(\frac{2y}{b}\right)^2} \tag{21}$$

$$\frac{\mathrm{d}\Gamma}{\mathrm{d}y} = -\frac{4\Gamma_0 y}{b^2}\left(\sqrt{1 - \left(\frac{2y}{b}\right)^2}\right)^{-1} \tag{22}$$

$$\therefore w\left(y_0\right) = -\frac{\Gamma_0}{2b} \tag{23}$$

Where - point is the mid point of the wingspan. The lift of the finite wing is:

$$L = \int_{\frac{-b}{2}}^{\frac{b}{2}} \left(L\left(y\right)\right)\mathrm{d}y = \rho V_\infty \Gamma_0 \int_{\frac{-b}{2}}^{\frac{b}{2}} \sqrt{1 - \left(\frac{2y}{b}\right)^2}\,\mathrm{d}y = \frac{1}{4}\rho\Gamma_0 b\pi \tag{24}$$

$$C_L = \frac{L}{\frac{1}{2}\rho V_\infty^2 S} = \frac{\Gamma_0 b\pi}{2V_\infty S} \tag{25}$$

It is usually hard to calculated the lift force of the whole wing in the three dimensional world. So, it is much more easier just to consider slicing the wing into cross-sections. But we can't just add up all the independently calculated forces of each cross-sections because this approximation is incorrect. In practice, each cross-section of the wing will influence its neighbouring one. The lifting-line theory correct part of the errors by introducing the interactions between the wing slices.

To maximize the efficiency of the wing, we must maximize the lift force exerted on the wing surface. To achieve that, we must minimize the downwash at the wing tips. One of the way to do so is to change the wing tip by adding a winglet.

Part 1 - Experimental Data Processing

Description of the experimental apparatus, the experimental procedure and sources of error. Explanation on why negative pressures are measured

The goal of this experiment is to measure the pressure around the airfoil. Pressure tappings are located on the upper and lower surfaces of the airfoil. These tappings are connected to a manometer using tubes. The multi-tube manometer is filled with coloured water, and half of it is connected to the pressure tappings of the airfoil and measures the pressure different point on the its surfaces, and the other half is left unconnected, and measures the atmospheric pressure of the room. The airfoil is placed in an air tunnel, and can be rotated with the help of a remote controlled stepper motor. Next, the wind tunnel velocity (free stream total) can be calculated using P_{tot} which is measured with a pitot tube inside the wind tunnel, P_{inf} which is measured by a pressure tapping on the wall of the wind tunnel, and the air density which is given. The sources of errors can come from an air leakage, an imprecise angle of attack, non-negligible drag and lift forces on the support of the wing (test rig). All the measured pressures are inferior than P_{atm} which is measured by the tube 21, so they are all negative with respect to the measured atmospheric pressure - this creates a vacuum at the top and bottom surfaces of the airfoil. However, when the angle of attack is between 0 and 18 degrees, the pressure at the top is lower than the pressure at the bottom, lifting the airfoil upwards.

Determination of the free stream velocity, U_∞, and the Reynolds number, Re

The free stream can be calculated as such:

$$U_\infty = \sqrt{\frac{2}{\rho}\left(P_{tot} - P_{inf}\right)} = \sqrt{\frac{2}{1.23}\left(|42 - 71|\right) \cdot 9.80638} = 20.50\,\mathrm{m\,s^{-1}} \tag{26}$$

The Reynolds number can be calculated as such:

$$Re = \frac{\rho v l}{\mu} = \frac{1.23 \cdot 6.87 \cdot 0.15}{1.938 \cdot 10^{-5}} = 63919 \tag{27}$$

Determination of pressure coefficient, c_p, for each angle of attack of the upper and lower surface with tabulated data

	Upper surface										Lower surface									
Angle	1	3	5	7	9	11	13	15	17	19	2	4	6	8	10	12	14	16	18	20
-9	412	398	370	360	355	353	353	355	360	360	280	285	300	310	322	332	380	345	350	358
-7,2	412	380	355	348	348	348	350	352	354	360	315	305	312	317	325	335	380	348	350	357
-5,4	403	360	342	338	342	343	347	350	356	360	345	322	324	325	331	338	380	348	350	356
-3,6	385	352	340	338	346	350	354	350	355	360	370	350	346	345	348	350	382	348	350	356
-1,8	360	318	316	317	330	338	344	350	355	360	392	355	348	345	343	345	385	358	352	357
0	325	290	300	305	325	336	341	350	355	360	412	371	360	355	350	351	390	355	355	360
1,8	281	260	281	295	320	331	340	348	350	360	420	385	362	355	350	348	382	350	350	360
3,6	240	230	261	286	313	330	339	346	355	360	422	398	381	372	365	360	394	360	360	362
5,4	190	198	250	275	310	325	338	345	350	361	424	395	380	370	360	356	396	362	360	363
7,2	131	167	243	265	304	322	335	343	352	361	420	410	394	386	372	370	394	362	361	363
9	87	120	230	255	300	322	334	343	355	361	412	416	402	391	380	372	400	365	363	363
10,8	45	109	215	248	298	320	333	344	353	358	405	420	408	398	382	378	400	370	364	363
12,6	7	95	205	242	305	320	334	344	351	354	392	422	412	402	388	380	402	370	364	363
14,4	275	284	286	283	291	290	297	301	310	312	407	402	390	380	368	360	386	350	342	340
16,2	278	281	286	285	293	290	295	300	305	310	410	405	391	381	369	360	386	350	340	337
18	282	290	292	291	299	293	295	297	300	303	410	405	391	381	369	360	384	348	339	333

Figure 6: Measured pressure (in mmH20) of the tappings at each angle.

	Upper surface										Lower surface									
Angle	1	3	5	7	9	11	13	15	17	19	2	4	6	8	10	12	14	16	18	20
-9	-15	-29	-57	-67	-72	-74	-74	-72	-67	-67	-147	-142	-127	-117	-105	-95	-47	-82	-77	-69
-7,2	-15	-47	-72	-79	-79	-79	-77	-75	-73	-67	-112	-122	-115	-110	-102	-92	-47	-79	-77	-70
-5,4	-24	-67	-85	-89	-85	-84	-80	-77	-71	-67	-82	-105	-103	-102	-96	-89	-47	-79	-77	-71
-3,6	-42	-75	-87	-89	-81	-77	-73	-77	-72	-67	-57	-77	-81	-82	-79	-77	-45	-79	-77	-71
-1,8	-67	-109	-111	-110	-97	-89	-83	-77	-72	-67	-35	-72	-79	-82	-84	-82	-42	-69	-75	-70
0	-102	-137	-127	-122	-102	-91	-86	-77	-72	-67	-15	-56	-67	-72	-77	-76	-37	-72	-72	-67
1,8	-146	-167	-146	-132	-107	-96	-87	-79	-77	-67	-7	-42	-65	-72	-77	-79	-45	-77	-77	-67
3,6	-187	-197	-166	-141	-114	-97	-88	-81	-72	-67	-5	-29	-46	-55	-62	-67	-33	-67	-67	-65
5,4	-237	-229	-177	-152	-117	-102	-89	-82	-77	-66	-3	-32	-47	-57	-67	-71	-31	-65	-67	-64
7,2	-296	-260	-184	-162	-123	-105	-92	-84	-75	-66	-7	-17	-33	-41	-55	-57	-33	-65	-66	-64
9	-340	-307	-197	-172	-127	-105	-93	-84	-72	-66	-15	-11	-25	-36	-47	-55	-27	-62	-64	-64
10,8	-382	-318	-212	-179	-129	-107	-94	-83	-74	-69	-22	-7	-19	-29	-45	-49	-27	-57	-63	-64
12,6	-420	-332	-222	-185	-122	-107	-93	-83	-76	-73	-35	-5	-15	-25	-39	-47	-25	-57	-63	-64
14,4	-152	-143	-141	-144	-136	-137	-130	-126	-117	-115	-20	-25	-37	-47	-59	-67	-41	-77	-85	-87
16,2	-149	-146	-141	-142	-134	-137	-132	-127	-122	-117	-17	-22	-36	-46	-58	-67	-41	-77	-87	-90
18	-145	-137	-135	-136	-128	-134	-132	-130	-127	-124	-17	-22	-36	-46	-58	-67	-43	-79	-88	-94

Figure 7: Water height differences.

	Upper surface										Lower surface									
Angle	1	3	5	7	9	11	13	15	17	19	2	4	6	8	10	12	14	16	18	20
-9	-147,1	-284,4	-559,0	-657,0	-706,1	-725,7	-725,7	-706,1	-657,0	-657,0	-1441,5	-1392,5	-1245,4	-1147,3	-1029,7	-931,6	-460,9	-804,1	-755,1	-676,6
-7,2	-147,1	-460,9	-706,1	-774,7	-774,7	-774,7	-755,1	-735,5	-715,9	-657,0	-1098,3	-1196,4	-1127,7	-1078,7	-1000,3	-902,2	-460,9	-774,7	-755,1	-686,4
-5,4	-235,4	-657,0	-833,5	-872,8	-833,5	-823,7	-784,5	-755,1	-696,3	-657,0	-804,1	-1029,7	-1010,1	-1000,3	-941,4	-872,8	-460,9	-774,7	-755,1	-696,3
-3,6	-411,9	-735,5	-853,2	-872,8	-794,3	-755,1	-715,9	-755,1	-706,1	-657,0	-559,0	-755,1	-794,3	-804,1	-774,7	-755,1	-441,3	-774,7	-755,1	-696,3
-1,8	-657,0	-1068,9	-1088,5	-1078,7	-951,2	-872,8	-813,9	-755,1	-706,1	-657,0	-343,2	-706,1	-774,7	-804,1	-823,7	-804,1	-411,9	-676,6	-735,5	-686,4
0	-1000,3	-1343,5	-1245,4	-1196,4	-1000,3	-892,4	-843,3	-755,1	-706,1	-657,0	-147,1	-549,2	-657,0	-706,1	-755,1	-745,3	-362,8	-706,1	-706,1	-657,0
1,8	-1431,7	-1637,7	-1431,7	-1294,4	-1049,3	-941,4	-853,2	-774,7	-755,1	-657,0	-68,6	-411,9	-637,4	-706,1	-755,1	-774,7	-441,3	-755,1	-755,1	-657,0
3,6	-1833,8	-1931,9	-1627,9	-1382,7	-1117,9	-951,2	-863,0	-794,3	-706,1	-657,0	-49,0	-284,4	-451,1	-539,4	-608,0	-657,0	-323,6	-657,0	-657,0	-637,4
5,4	-2324,1	-2245,7	-1735,7	-1490,6	-1147,3	-1000,3	-872,8	-804,1	-755,1	-647,2	-29,4	-313,8	-460,9	-559,0	-657,0	-696,3	-304,0	-637,4	-657,0	-627,6
7,2	-2902,7	-2549,7	-1804,4	-1588,6	-1206,2	-1029,7	-902,2	-823,7	-735,5	-647,2	-68,6	-166,7	-323,6	-402,1	-539,4	-559,0	-323,6	-637,4	-647,2	-627,6
9	-3334,2	-3010,6	-1931,9	-1686,7	-1245,4	-1029,7	-912,0	-823,7	-706,1	-647,2	-147,1	-107,9	-245,2	-353,0	-460,9	-539,4	-264,8	-608,0	-627,6	-627,6
10,8	-3746,0	-3118,4	-2079,0	-1755,3	-1265,0	-1049,3	-921,8	-813,9	-725,7	-676,6	-215,7	-68,6	-186,3	-284,4	-441,3	-480,5	-264,8	-559,0	-617,8	-627,6
12,6	-4118,7	-3255,7	-2177,0	-1814,2	-1196,4	-1049,3	-912,0	-813,9	-745,3	-715,9	-343,2	-49,0	-147,1	-245,2	-382,4	-460,9	-245,2	-559,0	-617,8	-627,6
14,4	-1490,6	-1402,3	-1382,7	-1412,1	-1333,7	-1343,5	-1274,8	-1235,6	-1147,3	-1127,7	-196,1	-245,2	-362,8	-460,9	-578,6	-657,0	-402,1	-755,1	-833,5	-853,2
16,2	-1461,2	-1431,7	-1382,7	-1392,5	-1314,1	-1343,5	-1294,4	-1245,4	-1196,4	-1147,3	-166,7	-215,7	-353,0	-451,1	-568,8	-657,0	-402,1	-755,1	-853,2	-882,6
18	-1421,9	-1343,5	-1323,9	-1333,7	-1255,2	-1314,1	-1294,4	-1274,8	-1245,4	-1216,0	-166,7	-215,7	-353,0	-451,1	-568,8	-657,0	-421,7	-774,7	-863,0	-921,8

Figure 8: Static pressure at each taps in Pa.

	Upper surface										Lower surface									
Angle	1	3	5	7	9	11	13	15	17	19	2	4	6	8	10	12	14	16	18	20
-9	2,1	1,6	0,5	0,2	-0,0	-0,1	-0,1	-0,0	0,2	0,2	-2,9	-2,7	-2,1	-1,7	-1,3	-0,9	0,9	-0,4	-0,2	0,1
-7,2	2,1	0,9	-0,0	-0,3	-0,3	-0,3	-0,2	-0,2	-0,1	0,2	-1,6	-1,9	-1,7	-1,5	-1,2	-0,8	0,9	-0,3	-0,2	0,0
-5,4	1,8	0,2	-0,5	-0,7	-0,5	-0,5	-0,3	-0,2	0,0	0,2	-0,4	-1,3	-1,2	-1,2	-0,9	-0,7	0,9	-0,3	-0,2	0,0
-3,6	1,1	-0,2	-0,6	-0,7	-0,4	-0,2	-0,1	-0,2	-0,0	0,2	0,5	-0,2	-0,4	-0,4	-0,3	-0,2	1,0	-0,3	-0,2	0,0
-1,8	0,2	-1,4	-1,5	-1,5	-1,0	-0,7	-0,5	-0,2	-0,0	0,2	1,4	-0,0	-0,3	-0,4	-0,5	-0,4	1,1	0,1	-0,2	0,0
0	-1,2	-2,5	-2,1	-1,9	-1,2	-0,8	-0,6	-0,2	-0,0	0,2	2,1	0,6	0,2	-0,0	-0,2	-0,2	1,3	-0,0	-0,0	0,2
1,8	-2,8	-3,6	-2,8	-2,3	-1,4	-0,9	-0,6	-0,3	-0,2	0,2	2,4	1,1	0,2	-0,0	-0,2	-0,3	1,0	-0,2	-0,2	0,2
3,6	-4,4	-4,8	-3,6	-2,7	-1,6	-1,0	-0,6	-0,4	-0,0	0,2	2,5	1,6	0,9	0,6	0,3	0,2	1,4	0,2	0,2	0,2
5,4	-6,3	-6,0	-4,0	-3,1	-1,7	-1,2	-0,7	-0,4	-0,2	0,2	2,6	1,5	0,9	0,5	0,2	0,0	1,5	0,2	0,2	0,3
7,2	-8,5	-7,2	-4,3	-3,5	-2,0	-1,3	-0,8	-0,5	-0,2	0,2	2,4	2,0	1,4	1,1	0,6	0,5	1,4	0,2	0,2	0,3
9	-10,2	-9,0	-4,8	-3,8	-2,1	-1,3	-0,8	-0,5	-0,0	0,2	2,1	2,3	1,7	1,3	0,9	0,6	1,7	0,3	0,3	0,3
10,8	-11,8	-9,4	-5,3	-4,1	-2,2	-1,4	-0,9	-0,5	-0,1	0,1	1,9	2,4	2,0	1,6	1,0	0,8	1,7	0,5	0,3	0,3
12,6	-13,2	-9,9	-5,7	-4,3	-1,9	-1,4	-0,8	-0,5	-0,2	-0,1	1,4	2,5	2,1	1,7	1,2	0,9	1,7	0,5	0,3	0,3
14,4	-3,1	-2,7	-2,7	-2,8	-2,5	-2,5	-2,2	-2,1	-1,7	-1,7	1,9	1,7	1,3	0,9	0,5	0,2	1,1	-0,2	-0,5	-0,6
16,2	-3,0	-2,8	-2,7	-2,7	-2,4	-2,5	-2,3	-2,1	-1,9	-1,7	2,0	1,9	1,3	0,9	0,5	0,2	1,1	-0,2	-0,6	-0,7
18	-2,8	-2,5	-2,4	-2,5	-2,2	-2,4	-2,3	-2,2	-2,1	-2,0	2,0	1,9	1,3	0,9	0,5	0,2	1,1	-0,3	-0,6	-0,9
x/c	0,0	0,0	0,1	0,1	0,3	0,4	0,5	0,7	0,8	0,9	0,0	0,1	0,1	0,2	0,3	0,4	0,5	0,6	0,8	0,9
x in mm	0,8	3,8	11,4	19,1	38,0	62,0	80,7	101,4	122,0	137,1	1,5	7,7	15,3	22,8	41,1	59,4	77,7	96,0	114,3	129,6

Figure 9: Pressure coefficients at the tappings at each angle.

The pressure coefficient can be determined by the following formula:

$$C_p = \frac{p - p_\infty}{\frac{1}{2}\rho V_\infty^2} \tag{28}$$

$$p_\infty = -71 \cdot 9.80638 = -696.253\,\text{Pa} \text{ and } V_\infty - 20.50\,\text{m}\,\text{s}^{-1} \tag{29}$$

Plot of the variation along the chord of c_p at $\alpha = 0°$, $4°$ and $14°$ and discussion

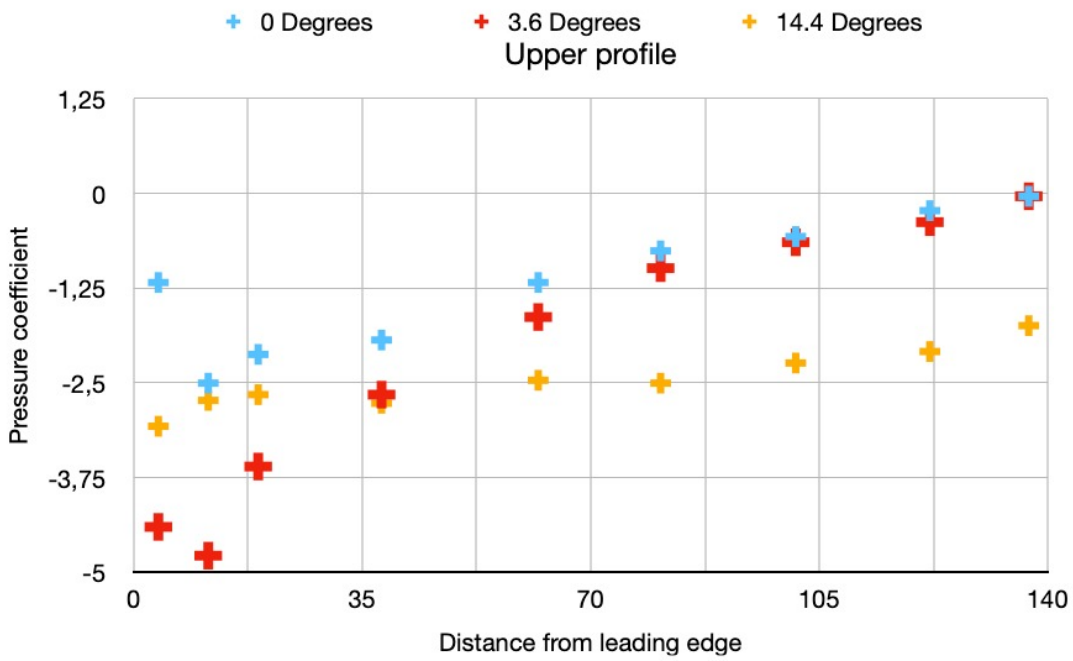

Figure 10: Upper profile variation.

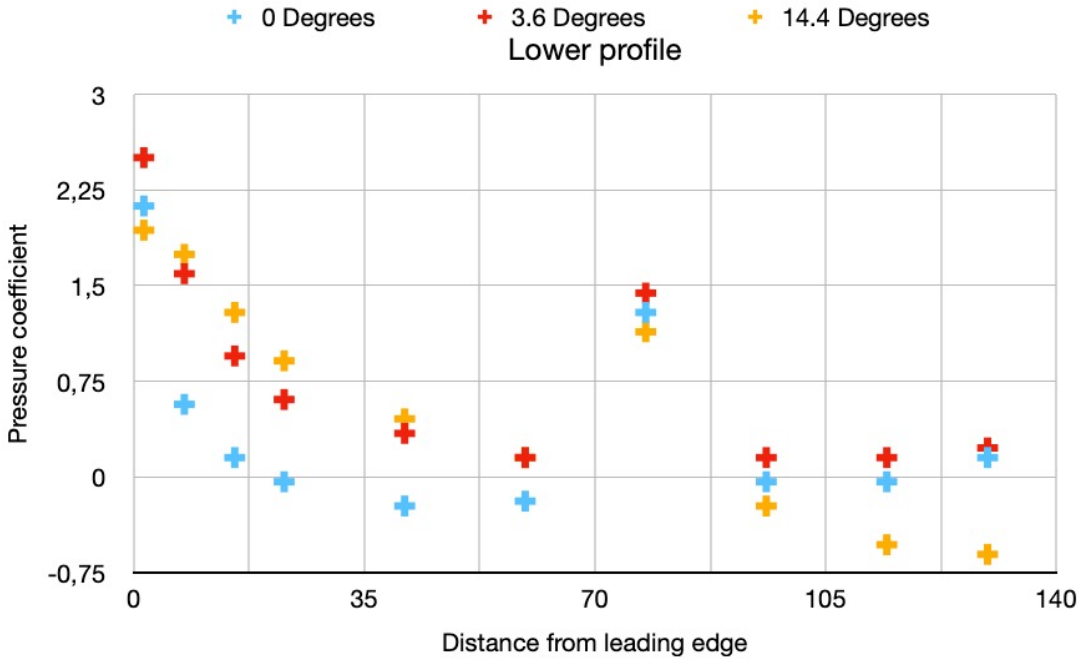

Figure 11: Lower profile variation.

We can see that for the upper profile, at angles of attack of 0° and 3.6°, the pressure coefficient along the chord are negative which represent a suction, apart from the last data point which is positive. This corresponds to the typical pressure distribution given in Fig.8. However, for the 14° angle of attack, we can see that the last data point is negative. We can see that for the lower profile, for a 3.6° angle of attack, the pressure coefficients are always positive, which means that there is a compression region lifting the airfoil upwards. For a 0° angle of attack, the pressure coefficient is positive then turns negative before turning positive again, and is very close to 0 along the chord, meaning the compression or suction generated will be significantly smaller so the lift will be smaller. Finally, at an angle of attack of 14.4°, the pressure coefficient does not turn positive towards the end of the chord like for the two other angles, indicating the presence of a suction region. We can also see that at the angle of attack of 14.4°, the pressure coefficients at the end of the chord in the upper profile does not get closer to 0 like there would be in a typical pressure distribution. Finally we can see that until 35 mm from the leading edge, at a 3.6° angle of attack, the pressure coefficient is approximately two times higher than at a 14.4° angle of attack.

Part 2 - Conformal Mapping

Shape change of the cylinder when the parameters, x_c, y_c and λ are varied

Varying the value of λ between 0 and 1 compressed the cylinder into an elliptical shape and approached the shape of a line with length $4r$ at $\lambda = 1$. For values greater than 1, the shape produced was an ellipse and an increase in λ provided a scaling effect. Changing x_c would change the shape of the cylinder from elliptical to a symmetrical tear drop shape (aerofoil shape), with one edge becoming more pinched and the other more rounded. Changing x_c when $\lambda < 1$ would pinch the right side, whereas for $\lambda > 1$ it would pinch the left side. Changing y_c would skew the aerofoil into a curved shape, becoming unsymmetrical. This would result in one of the profiles of the wing becoming concave.

Determination of the values of x_c and y_c

As our airfoil is uncambered (denoted by the 00 in NACA-0012), hence, our value of y_c is 0. After iteratively finding values of λ and x_c, the values of $\lambda = \sqrt{122}/10$ and $x_c = 0.06$. A NACA scaling factor of 4.43 with NACA shift x of -2.24 yielded a shape closely matching the grey profile. This can be seen below.

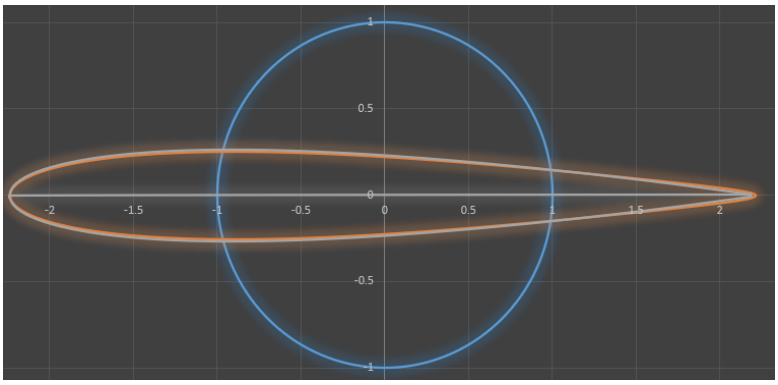

Figure 12: Matching conformally mapped aerofoil with NACA-0012 aerofoil.

Graphically estimating the chord, c, of this aerofoil, we attain a value of approximately 4.8. The

maximum thickness is approximated to to be around 0.44.

Determination of the lift, L, and a plot of the lift coefficient, c'_L, of the aerofoil as a function of the angle of incidence

$$\Gamma = 4\pi R U_\infty \sin a \tag{30}$$

$$L = \rho U_\infty \Gamma = 4\pi R \rho U_\infty^2 \sin a \tag{31}$$

$$c'_L = \frac{L}{\frac{1}{2}\rho U_\infty^2 c} = \frac{4\pi R \rho U_\infty^2 \sin a}{\frac{1}{2}\rho U_\infty^2 c} = \frac{4\pi R \sin a}{c} \tag{32}$$

$R = 1$ and $c = 3.6$. Hence:

$$c'_L = \frac{4\pi}{3.6} \sin a \tag{33}$$

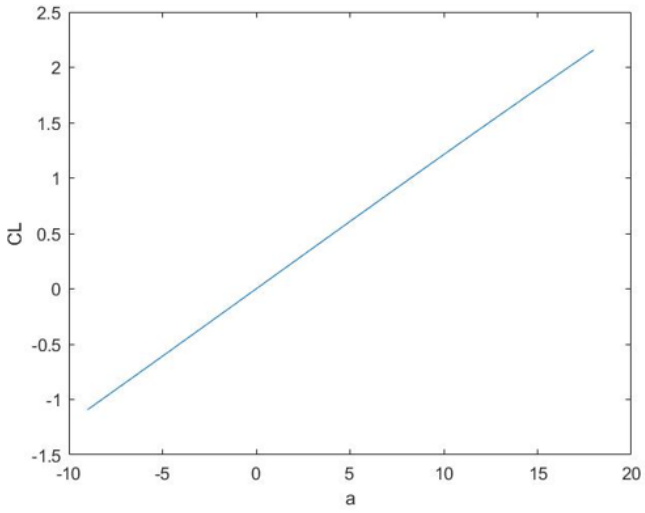

Figure 13: Plot of Eq.33.

The plot in Fig.13 is, as expected, a straight line. We know from Eq.33 that it is a sine function with a scalar factor. We also know from the small angle approximation that $\sin a \approx a$ for small a, leading to our lift coefficient being: $c'_L = \frac{8\pi}{3.6}a$, which is a straight line with a fixed gradient.

Compare the plot of the lift coefficient, c_L', with that obtained from experimental analysis. Discuss on the validity of conformal mapping over the range of angles investigated

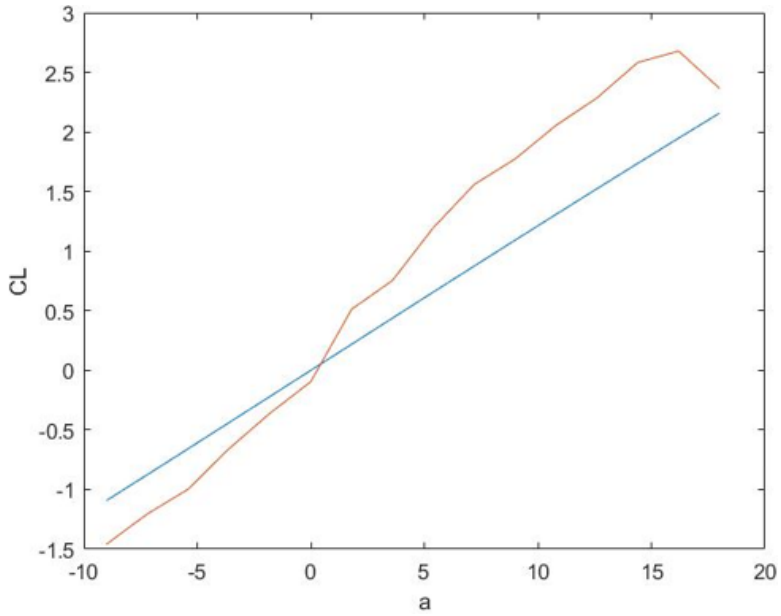

Figure 14: Plot of calculated c_L (blue) and of experimental c_L (red).

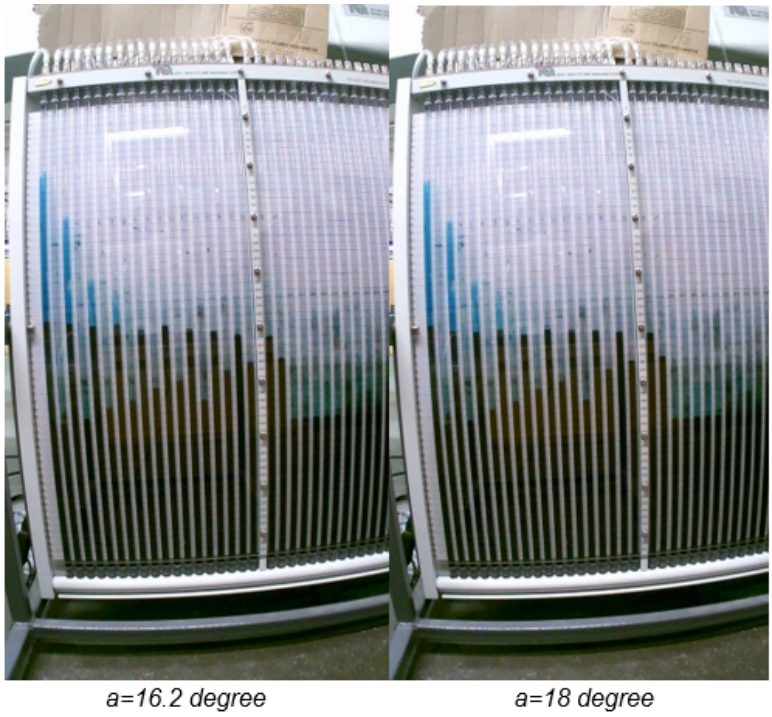

Figure 15: Manometer values for $a = 16.2°$ (left) and $a = 18°$ (right).

In general, conformal mapping is accurate to use. The two lines do not completely overlap, but the two lines are very close to each other before being intercepted, as no flow separation occurs. After the intercept point, the experimental c_L is still on the track of the theoretical c_L, but when the incident angle is between 16.2° and 18°, the experimental c_L suddenly drops. This is because when $a = 16.2° - 18°$, a stall occurs and flow separation occurs. When a is greater than the critical angle

of attack, boundary layer separation will occur on the upper surface of the wing. This is due to the existence of an unfavourable pressure gradient and wall stress equals zero at the flow separation point. As a result, the suction pressure is lost and the pressure difference will decrease and the lift will drop. From the experimental data, it can be observed that the pressure difference decreases. When a is between 16.2° and 18°, the pressure difference drops suddenly, which means that flow separation has occurred.